Comparative analysis of rabies pathogenic and vaccine strains detection by RIG-I-like receptors

Wahiba Aouadi, Valérie Najburg, Rachel Legendre, Hugo Varet, Lauriane Kergoat, Frédéric Tangy, Florence Larrous, Anastassia V Komarova, Hervé Bourhy

Microbes and Infection xxx (xxxx) xxx

Contents lists available at ScienceDirect

Microbes and Infection

journal homepage: www.elsevier.com/locate/micinf

Original article

Comparative analysis of rabies pathogenic and vaccine strains detection by RIG-I-like receptors

Wahiba Aouadi [a], Valérie Najburg [b], Rachel Legendre [c], Hugo Varet [c], Lauriane Kergoat [a], Frédéric Tangy [b], Florence Larrous [a], Anastassia V. Komarova [d,**], Hervé Bourhy [a,*]

[a] Institut Pasteur, Université Paris Cité, Lyssavirus Epidemiology and Neuropathology Unit, 75015 Paris, France
[b] Institut Pasteur, Université Paris Cité, Vaccines-innovation Laboratory, 75015 Paris, France
[c] Institut Pasteur, Université Paris Cité, Hub Bioinformatics, and Biostatistics, 75015 Paris, France
[d] Institut Pasteur, Université Paris Cité, Interactomics, RNA and Immunity Laboratory, 75015 Paris, France

ARTICLE INFO

Article history:
Received 21 November 2023
Accepted 6 March 2024
Available online xxx

Keywords:
Rabies virus (RABV)
Pathogenic RABV strain (Tha)
Vaccine RABV strain (SAD)
RLR (RIG-I-like receptor)
Retinoic acid-inducible gene-I (RIG-I)
5′ copy-back defective interfering (5′cb DI) viral genome

ABSTRACT

Rabies virus (RABV) is a lethal neurotropic virus that causes 60,000 human deaths every year globally. RABV infection is characterized by the suppression of the interferon (IFN)-mediated antiviral response. However, molecular mechanisms leading to RABV sensing by RIG-I-like receptors (RLR) that initiates IFN signaling currently remain elusive. Here, we showed that RABV RNAs are primarily recognized by the RIG-I RLR, resulting in an IFN response in the infected cells, but this response varied according to the type of RABV used. Pathogenic RABV strain RNAs, Tha, were poorly detected in the cytosol by RIG-I and therefore caused a weak antiviral response. However, we revealed a strong IFN activity triggered by the attenuated RABV vaccine strain RNAs, SAD, mediated by RIG-I. We characterized two major 5′ copy-back defective interfering (5′cb DI) genomes generated during SAD replication. Furthermore, we identified an interaction between 5′cb DI genomes, and RIG-I correlated with a high stimulation of the type I IFN signaling. This study indicates that wild-type RABV RNAs poorly activate the RIG-I pathway, while the presence of 5′cb DIs in the live-attenuated vaccine strain serves as an intrinsic adjuvant that strengthens its efficiency by enhancing RIG-I detection thus strongly stimulates the IFN response.

1. Introduction

The innate immune response provides the first line of defense against viral infections. Pattern recognition receptors (PRRs) recognize the non-self-motifs within viral products known as pathogen-associated molecular patterns (PAMPs) that trigger the release of IFN and proinflammatory antiviral cytokines [1].

Among PRRs, RIG-I-like receptors (RLRs) are RNA sensors localized in the cytosol. This receptor family encompasses three members: RIG-I, melanoma differentiation-associated protein 5 (MDA5), and laboratory of genetics and physiology 2 (LGP2). RIG-I and MDA5 have two amino acid terminal domains, caspase activation, and recruitment (CARDs). Upon RNA binding to RIG-I or MDA5, CARD domains interact with mitochondrial antiviral signaling proteins (MAVS), mediate the downstream signal transduction and stimulate IFN release. IFN then activates neighboring cells *via* the JAK/STAT pathway, stimulating the expression of IFN-stimulated genes (ISGs). The LGP2 on the other hand, lacks the CARD domain, and instead fine-tunes the immune response by inhibiting RIG-I and supporting the MDA5 sensing [2,3].

RIG-I is the major sensor for RNA viruses belonging to Orthomyxoviridae (Influenza A virus), Paramyxoviridae (Measles virus), and Rhabdoviridae (Vesicular stomatitis virus) [4,5]. MDA5 detects members of Picornaviridae (encephalomyocarditis virus), Coronaviridae (SARS-CoV-2), and *Calciviridae* (murine norovirus-1) [6,7].

Molecular characterization of RIG-I reveals its interaction with 5′-triphosphate double-stranded RNA (dsRNA) which is inhibited by the capping of the 5′-end [8,9]. MDA5 recognizes the internal duplex structures within high molecular weight dsRNAs in virus-infected cells [10,11].

There are several types of viral RNA structures listed as being detected by RIG-I [5,12,13]. Among them, the 5′cb DI genomes are

* Corresponding author.
** Corresponding author.
E-mail addresses: anastasia.komarova@pasteur.fr (A.V. Komarova), herve.bourhy@pasteur.fr (H. Bourhy).

https://doi.org/10.1016/j.micinf.2024.105321
1286-4579/

potent inducers of the innate immune response due to their double-stranded stem-loop-like structures harboring a 5′-triphosphate extremity [4,12,14,15]. While it has become clear that 5′cb DI genomes are potent inducers of the innate immune response, how 5′cb DI genomes are produced is currently not fully understood. What is known is that they are released when the viral polymerase detaches from the template (breakpoint position: BP) and attaches to the nascent strand (reinitiation site: RI), which is then copied back producing 3′-RNA terminus with perfect complementarity to its 5′-end [16].

RNA viruses have evolved synergistic strategies to counteract the host's innate immune response to sustain infection. This is the case for RABV, one of the most lethal neurotropic zoonotic viruses causing acute encephalitis in mammals in developing countries and resulting in an estimated 60,000 human deaths every year globally [17]. RABV belongs to the Rhabdoviridae family, *Lyssavirus* genus, and possesses a negative-sense single-stranded RNA genome encoding five proteins: nucleoprotein (N), phosphoprotein (P), matrix protein (M), glycoprotein (G), and polymerase (L). N, P, and M proteins are major antagonists of the host type-I IFN pathway and enable viral evasion of the innate antiviral response. N counteracts the activation of the RIG-I sensor [18,19]. P inhibits the expression of IFN genes and ISGs by i) blocking the phosphorylation of IFN regulatory factors (IRF) 3 and IRF7; ii) preventing the IFN-I stimulated JAK/STAT pathway by retaining STATs in the cytoplasm; and iii) antagonizing cytokine activated STAT3-STAT1 heterodimers [20–23]. RABV M targets RelAP43, a member of the NF-κB family, thus inducing inhibition of NF-κB signaling and reducing the expression of IFN-β genes [24,25]. Further, the M protein cooperates with P to modulate the JAK-STAT pathway [26]. Additionally, electron microscopy of the RABV and VSV L protein showed the presence of the methyltransferase catalytic domain [27,28]. RNA methylation occurs on nascent RNAs at N7 and/or 2′O positions during the viral mRNA capping process [29,30]. The N7 methylation is required for the translation of viral mRNA while the 2′O methylation facilitates evasion of viral RNA recognition by RIG-like receptors [31,32].

While it has become clear that RABV viral proteins enable viral evasion of the innate antiviral response, few studies have addressed the RLR recognition of RABV RNAs upon infection. Indeed, *in vitro* studies using genetically engineered RABV (SAD ΔPLP), which expresses little P due to a change in the gene order in the viral genome, have shown RLR's efficient induction of IFN release [9]. In this case, RNAs isolated from RABVΔP did induce IFN expression in RIG-I overexpressing cells and this effect was strongly inhibited by the RIG-I dominant-negative mutant. Moreover, the dephosphorylation of viral RNA suppresses IFN induction, thus suggesting that RABV 5′-pppRNAs are specifically sensed by RIG-I and as a result, trigger the IFN response [9].

In the present study, we compared molecular patterns of RLR-specific RNA ligands induced by an RABV field isolate and a vaccine strain. We used the previously validated RLR affinity purification approach combined with NGS [14,15,33,34] and identified the RNA molecular signatures on RIG-I and MDA5 during RABV replication. We demonstrated that IFN response, induced by RABV, was mediated by RIG-I. Further, 5′cb DI viral genomes, produced by the RABV live-attenuated vaccine strain, were sensed by RIG-I, resulting in a strong activation of the IFN response.

2. Material and methods

2.1. Virus and cells

SK-N-SH (human neuroblastoma, ATCC-HTB-11), and HEK293 (human embryonic kidney, ATCC CRL-1573) were maintained in DMEM supplemented with 10% calf serum. ISRE reporter cell line (STING37) and human HEK293 (293) cells stably expressing the 1-STrEP-tagged RLRs (1-STrEP-RLRs) RIG-I, MDA5, or LGP2, or the protein Cherry (negative control) [15,35] were maintained in DMEM supplemented with 10% calf serum containing G418 at 400 μg/ml (#G8168, SIGMA, St. Louis, Missouri).

The rabies virulent cell culture-adapted canine RABV field isolate, 8743 THA (Tha; EVAg collection, Ref-SKU: 014V-02106; GenBank accession: n°EU293121.1) was isolated from a man bitten by a dog in Thailand.

The rabies vaccine SAD B19 Bern-C strain was obtained from EVAg collection (Ref-SKU: 014V-02293; Genbank accession number GU992311.1).

2.2. Immunostimulation assay on ISRE reporter cell line and HEK 293 cells

Total virus-RNAs were extracted from SK-N-SH infected cells. ISRE reporter assays with extracted total and 5′cb DI-1668 or DI-2170 RNAs were performed using the ISRE reporter cell line [35]. The IFN-β reporter assay was assessed by transient transfection of HEK293 and ST-LGP2 cells using a reporter plasmid expressing luciferase under the control of the IFN-β promoter. Short 5′-PPP-bearing home-made RNA molecules, low molecular weight (LMW, (#tlrl-picw, Invivogen)) and high molecular weight (HMW, (#tlrl-pic, Invivogen)) poly(I:C) were used as positive controls.

2.3. RNAi experiments

ISRE reporter cell line cells were transfected with small interfering RNAs: si-RIG-I (Horizon Discovery #L-012411-00-0005), si-MDA5 (#L-013041-00-0005), or non-targeting (si-control, #D-001810-10-05) and incubated for 24h before transfection with RNA ligands to perform the ISRE-reporter assays.

2.4. Reverse transcription-PCR analysis

Total RNA was extracted from SK-N-SH and ST-RLR cells infected with THA or SAD RABV strains. At the cDNA step, viral genome and DI-RNA fragments were amplified using universal or virus strain-specific primers presented in Table S7. Corresponding amplified DNA products were then analyzed on an agarose gel.

2.5. Western blot and antibodies

Protein extracts were resolved by SDS-polyacrylamide gel electrophoresis on 4–12 % gradient NUPAGE gel (Invitrogen) with MOPS running buffer and transferred to cellulose membranes (GE Healthcare) with the Criterion Blotter system (Biorad). For this, the following antibodies were used: an anti-STrEP-Tag (#34850, Qiagen), a monoclonal anti-β-actin antibody (A5441, Sigma), and HRP-coupled anti-mouse (NA9310V, GE Healthcare) or anti-rabbit (RPN4301, GE Healthcare) were used as secondary antibodies. Peroxidase activity was visualized with an ECL Plus Western Blotting Detection System (#RPN2132, GE Healthcare).

2.6. Purification of ST-RLR/RNAs by affinity chromatography

ST-RLR cells were infected at a multiplicity of infection (MOI) of 0.5 by either Tha wild-type or SAD. The cells were harvested 24h post-infection and RLR-RNA complexes were pulled-down as previously described in Refs. [14,15,33,34]. RNAs bound to RLR were extracted with TRI reagent LS and resuspended in ultrapure RNase-free water. The quality of input and output RNAs was controlled on Bioanalyzer (Agilent, Santa Clara, California).

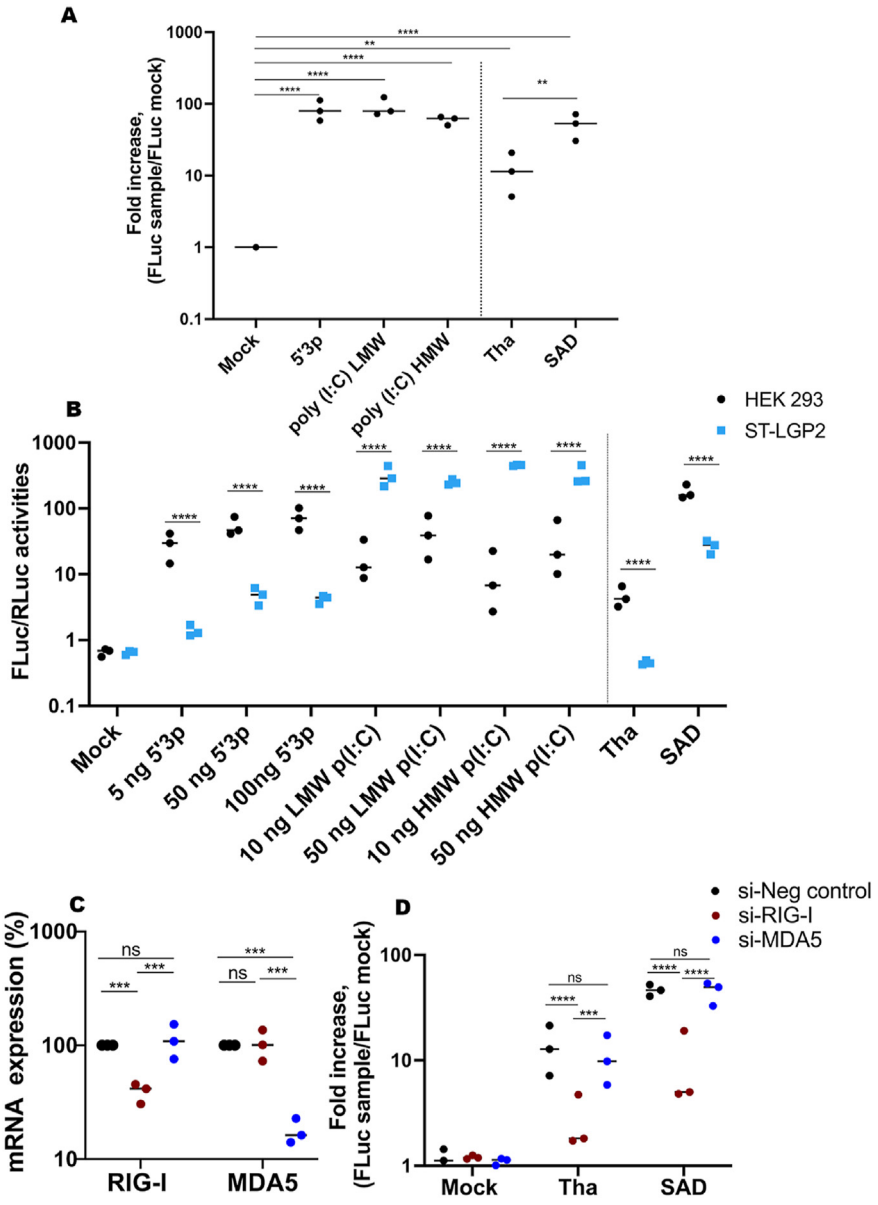

Fig. 1. RNAs purified from RABV-infected cells are immunoactive: Total RNA was purified from SK-N-SH cells infected with Tha or SAD for all experimental approaches presented in the figure. SK-N-SH cells were infected with Tha or SAD at an MOI of 0.5 for 72h, (**A**) 50 ng of total RNAs were transfected into ISRE-reporter cells, and firefly luciferase expression was monitored. (**B**) IFN-β promoter expression in HEK293 cells (black) or in HEK293 expressing one-Strep tagged-LGP2 ST-LGP2 (blue) transfected with 50 ng of Tha, SAD total RNAs or with each of the indicated synthetic RLR ligands. (**C**) Relative expression of *RIG-I* and *MDA5* mRNAs in ISRE-reporter cells silenced with non-targeting si-RNAs si-Negative control (black), targeting RIG-I (si-RIG-I in red) or MDA5 (si-MDA5 in blue). (**D**) The indicated silenced ISRE-reporter cells were transfected for 24h with 50 ng of total RNAs extracted from Tha- or SAD-infected cells followed by luciferase assay measurement. The results are represented as a fold increase of ISRE expression compared to Mock non-transfected cells. The experiments were performed three times and represented as a median. P values were calculated using one-way ANOVA with Tukey's multiple comparisons. Non-significant (n.s.) were indicated. *p < 0.05, **p < 0.01, ***p < 0.001, ****P < 0.0001.

2.7. Library preparation

RNA molecules extracted from input and output preparations were used for library preparation using the TruSeq stranded total RNA library prep kit (Illumina, San Diego, California), according to the manufacturer's instructions. The first step of poly-A RNA isolation was omitted to analyze all RNA species present. First, the RNAs were randomly fragmented and random primed reverse transcription was performed. dsDNA fragments were generated by second-strand DNA synthesis. To add specific, Illumina adapters, an adenine was added to the 3′ extremity followed by adapter ligation. The quality of all libraries was checked with the DNA-1000 kit (Agilent) on a 2100 Bioanalyzer and quantification was performed with Quant-It assays on a Qubit 1.0 fluorometer (Invitrogen). Sequencing was performed with the Illumina NextSeq500 system. Runs were carried out over 75 cycles, including seven indexing cycles, to obtain 75-bp single-end reads. Sequencing data were processed with Illumina Pipeline software (Casava version 1.9).

2.8. RLR binding analysis

Adapter sequences and low-quality sequences were removed from reads using cutadapt (version 3.2.). Only sequences at least 25 nt in length were considered for further analysis. Bowtie

(version 2.1.0 with –very-sensitive mode) was used for alignment on the reference genomes Tha and SAD, respectively. Coverage was obtained using BEDTools (version 2.17.0) with genomecov -d parameters [36]. Analyses were performed in R (version 4.0.3) and bioconductor using the "*ggplot2*" (version 3.3.3) and "*tidyr*" (version 1.1.3) packages as described previously [33]. The read coverage of each output sample was normalized by the mean read coverage of their input extracts. To obtain RLR binding, the normalized output samples were normalized by the mean of the negative control (mCherry samples triplicates), at each genomic position. The RLR bindings were plotted using R package "ggplot2". DI-tector v0.6 [37] was used to detect Rabies defectives RNAs with parameters set to the default (using bwa v0.7.17, bedtools v2.17.0 and samtools v1.9).

2.9. Statistical analysis

A one-way Analysis of variance (ANOVA) model was used to assess xxxx, and the replicate effect was included as a blocking factor. Pairwise comparisons were extracted using the "*emmeans*" R package to adjust the p-values for multiple testing using the Tukey method.

See the supplementary material for additional information.

3. Results

3.1. RNAs purified from RABV-infected cells are immunoactive

To determine whether RABV RNAs induce IFN-mediated antiviral response, we used the previously validated ISRE reporter cell line which is HEK293 cells stably expressing firefly luciferase under the control of a promoter sequence containing five IFN-Stimulated Response Elements (ISRE) [35]. Total RNA was extracted from human neuroblastoma cells (SK-N-SH) following infection with either the RABV field isolate (Tha) or the SAD vaccine strain at a MOI of 0.5. The extracted RNA was subsequently transfected into the ISRE reporter cell line. As expected, ISRE expression was induced when the reporter cells were transfected with classical RLR agonists: 5′-pppRNAs (5′3P), low molecular weight (LMW) poly(I:C), and high molecular weight (HMW) poly(I:C) (Fig. 1A). Interestingly, RNA molecules extracted from Tha and SAD-infected cells induced statistically significant ($p < 0.01$, one-way ANOVA using Tukey method) activation of ISRE promoter (Fig. 1A). In addition, RNA molecules extracted from SAD-infected cells showed a statistically significant stronger activation ($p = 0.007$) of ISRE expression than observed for the parent strain Tha.

3.2. RIG-I is the main sensor of RABV infection in HEK293 cells

LGP2 is the third member of the RLR family and it is known to both inhibit RIG-I and amplify MDA-5-dependent responses [2,3]. Therefore, to further evaluate the role of RIG-I and/or MDA5 in RABV RNA detection and IFN signaling, we used HEK293 cell line stably over-expressing One-STrEP-tagged LGP2 (ST-LGP2) [15]. We previously demonstrated that LGP2 overexpression enhances MDA5-and blocks RIG-I-specific activation of the IFN-β promoter signal, providing an approach to distinguish between RIG-I- and MDA5-specific RNA ligands [2]. We evaluated IFN-β expression in either ST-LGP2 or parental HEK293 cells transfected with positive control RLR-ligands (synthetic RNAs) and with RABV total RNAs extracted from Tha- or SAD-infected SK-N-SH cells together with reporter plasmid expressing firefly luciferase (Fluc) under the control of IFN-β promoter (Fig. 1B). As expected, we observed that the transfection of ST-LGP2 with RIG-I-specific 5′3P RNA significantly suppressed the expression of Fluc compared to the parental HEK293 cells, whereas the transfection of ST-LGP2 with MDA5-specific ligands (LMW or HMW poly(I:C)) increased the activity of the IFN-β promoter. Similarly, to 5′3P, Tha and SAD total RNA molecules transfected in HEK293 induced the IFN-β promoter activity, whereas ST-LGP2 transfected cells showed significant suppression of IFN signaling (Fig. 1B), indicating that RIG-I is mainly implicated in RABV RNA detection upon infection.

To explore in more detail the differential involvement of RLR (RIG-I or MDA5) in RABV RNA sensing, the ISRE reporter cell line was treated with siRNAs targeting RIG-I (si-RIG-I) or MDA5 (si-MDA5). Transient silencing of RIG-I and MDA5 significantly reduced the level of mRNA for RIG-I and MDA5 by ~61% and ~82% ($p \leq 0.001$), respectively as compared to si-Negative control cells (Fig. 1C). When the same cells were transfected with RABV RNAs, only RIG-I silenced reporter cells transfected with Tha or SAD total RNAs showed strongly impaired ISRE promoter activation ($p < 0.0001$), while MDA5 silencing did not affect signaling (Fig. 1D). Altogether, these results demonstrate that RIG-I is the main cytosolic PRR that detects RABV RNAs and mediates IFN signaling.

3.3. During Tha and SAD infections immunoactive RNA ligands bind to RIG-I and modulate an IFN response

To evaluate the IFN stimulation activity of RLR-bound ligands from RABV-infected cells, we used previously validated HEK293 cells (ST-RLRs) expressing STrEP-tagged RIG-I (ST-RIG-I) and MDA5 (ST-MDA5) [14,15,33,34].

First, we tested whether RLR overexpression would influence RABV infection. ST-RIG-I and ST-MDA5 cells were infected at different MOIs either with the pathogenic RABV Tha strain or the SAD vaccine strain and were then compared with the negative control ST-CH cell line expressing STrEP-tagged Red Fluorescent Protein Cherry (mCherry, or CH) [15]. We first detected the efficacy of RABV replication in ST-RLR cells. Specifically, the virus growth was monitored at 16, 24, and 48h post-infection by quantification of genomic RNA using qPCR (Fig. S1). Tha replicated less efficiently than SAD in ST-RLR cells, especially at MOI of 0.1. However, the viral replications of Tha and SAD were comparable at an MOI of 0.5 or 1 24h and 48h post-infection. Furthermore, replications of Tha and SAD were not altered in cells expressing additional copies of RIG-I or MDA5 compared to ST-CH negative control cells.

Then we evaluated the activity of RNA molecules bound to RLR. For this, ST-CH, ST-RIG-I, and ST-MDA5 cell lines were infected by either Tha or SAD at an MOI of 0.5 and harvested at 24h post-infection. The efficiency of mCherry, RIG-I, and MDA5 proteins pull-down was controlled by western blotting. A lower amount of MDA5 is observed in the MDA-5 overexpressing cell line (ST-MDA5) but remains functional (Fig. 2A) [15].

Subsequently, RNAs co-purified with RIG-I, MDA5, or mCherry and then were extracted and transfected into the ISRE reporter cell line to assess the activation of type I IFN signaling. The ISRE promoter activation was first controlled by transfecting synthetic RNAs into the ISRE reporter cell line. As above, 5′3P, HMW poly(I:C), and LMW poly(I:C) largely stimulated ISRE expression (Fig. 2B). These RLR-specific positive control ligands validated the sensitivity and specificity of our ISRE reporter assay. RIG-I-specific RNAs extracted from Tha-infected cells induced a slight but significant ($p = 0.029$, one-way ANOVA) stimulation of ISRE expression as compared to the negative control CH-specific RNAs (Fig. 2C). RIG-I-specific SAD RNA molecules induced a strong and significant ($p = 0.00007$, one-way ANOVA) ISRE promoter activity in a dose-dependent manner as compared to negative control CH-specific RNAs (Fig. 2D). For both viral strains, MDA5-specific RNAs showed no significant stimulation of the ISRE promoter activity (Fig. 2C&D).

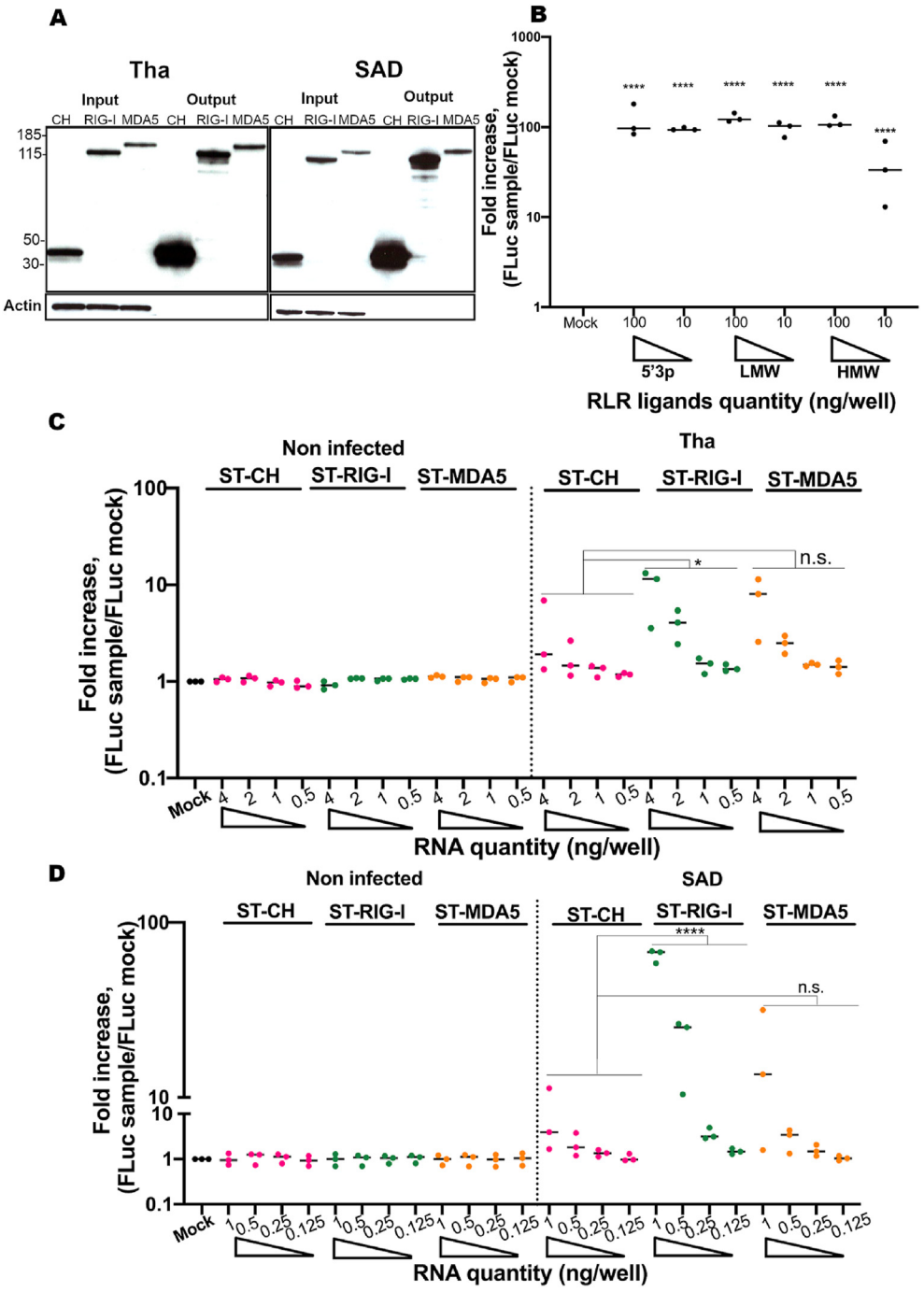

Fig. 2. Tha and SAD ligands bound to RIG-I are immunoactive. (**A**) Western blot analysis of RLR protein expression in ST-RLR infected cells. Total cell extracts (Input) were affinity-purified using Strep-tagged beads (Output). The Western blot was performed using α-STrEP-Tag (upper blot) or α-ß-actin (bottom blot) antibodies. Luciferase expression in ISRE-reporter cells transfected with a quantity of synthetic RLR ligand gradients (**B**), Tha (**C**)- or SAD-RNAs (**D**) co-purified with strep-tagged negative control cherry (CH represented in pink), RIG-I (green), or MDA5 (orange) extracted from ST-RLR cells-non-infected or infected at an MOI of 0.5 for 24h. Three biological replicates were performed for all experiments, and the data was represented as a median. The results are represented as a fold increase of ISRE expression compared to Mock (Lipofectamine only) cells. P values were calculated using one-way ANOVA with Tukey's multiple comparisons. Non-significant (n.s.) were indicated. *p < 0.05, **p < 0.01, ***p < 0.001, ****P < 0.0001.

These data suggest that RNA extracted from Tha- and SAD-infected cells present molecular patterns absent in non-infected cells and preferentially recognized by RIG-I.

3.4. The molecular pattern of RABV recognition by RIG-I and MDA5

To characterize RLR-bound RABV RNA ligands sequence, ST-RLRs cells were infected with Tha or SAD at an MOI of 0.5. The cells were harvested after 24h, and RLR complexes were purified using affinity chromatography. Total RNAs from input cell lysates, as well as RLRs-bound RNA output, were then extracted. Input and output RNAs were subjected to NGS followed by bioinformatics analysis using the previously described protocol [33,34]. We obtained between 12 and 90 million reads total per sample, with around 0.3 and 0.29% mapped to Tha and SAD genomes, respectively (Table S1). The fold change of RLR binding was obtained by normalizing: i) the mean

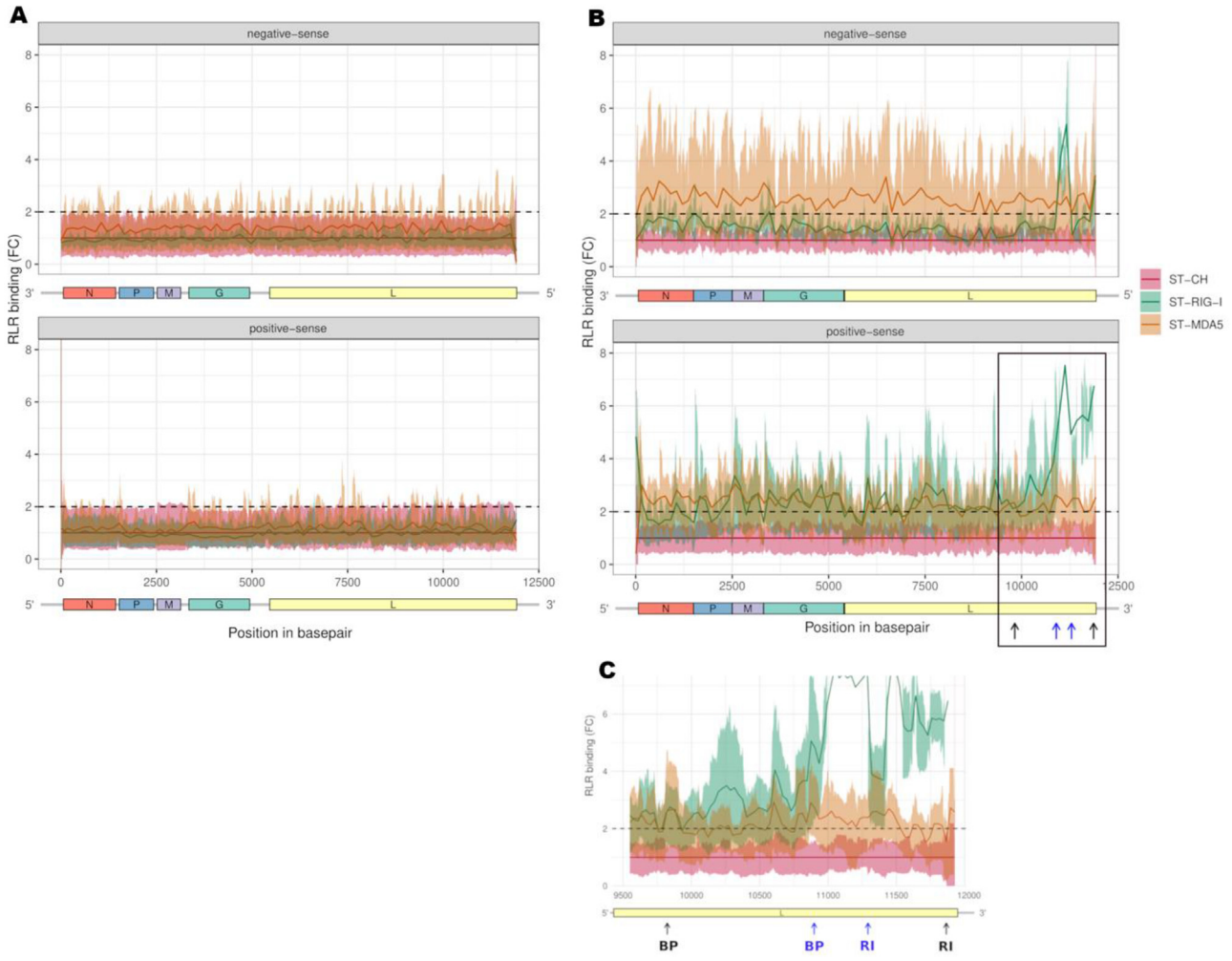

Fig. 3. Molecular pattern of RABV recognition by RIG-I and MDA5. RLR cells were infected with Tha or SAD at an MOI of 0.5 for 24h. (**A**) Tha or (**B**) SAD total RNAs extracts (Input) or co-purified (Output) with ST-CH (pink), ST-RIG-I (green), or ST-MDA5 (orange) are subjected to strand-specific NGS analysis. The read sequences obtained were mapped to Tha (**A**) or SAD (**B**) genome references in negative orientation (upper panel) or positive orientation (bottom panel) and are depicted on the y-axis as RLR binding fold change (FC) at each specific position along genome sequence represented on the x-axis. Schematic annotations of Tha (**A**) or SAD genome (**B**) underline the x-axis. (**C**) Zoom enlargement of the black framed panel B. Three independent experiments were represented as smooth curves. Black and blue arrows depicted the breakpoints, BP, and reinitiation sites, RI, for 5′ cb DI-2170 and 5′cb DI-1668, respectively. The fold change of RLR binding is obtained by i) normalizing the read coverage of output RNAs co-purified with RIG-I, MDA5, or CH by their input extract, ii) normalized read coverage of output samples divided by the mean of the coverage of negative control CH, at each genomic position.

Table 1
DI-tector results of NGS data analysis of SAD-infected cell.

5′ cb DI name	Samples	Length (nt)	BP position	RI position	ST-CH			ST-RIG-I			P values	ST-MDA5			p-values
					R1	R2	R3	R1	R2	R3		R1	R2	R3	
DI-2170	**Input**	2170	9823	11865	4	0	4	7	0	0	n.s.	0	0	4	n.s.
DI-1668		1668	10898	11292	2	0	0	0	3	0	n.s.	4	2	7	n.s.
DI-2170	**Output**	2170	9823	11865	0	0	0	14	2	0	n.s.	0	0	0	n.s.
DI-1668		1668	10898	11292	0	0	0	73	11	10	*	6	0	0	n.s.

Data sets were generated from RNA samples obtained from SAD-infected ST-Cherry (ST-CH), ST-RIG-I, or ST-MDA5 cells before (Input) or after purification (Output). R1, R2, and R3 are biological replicates. For each 5′cb DI, the breakpoint position (BP) and reinitiation site: (RI) are identified. P values were calculated using one-way ANOVA with Tukey's multiple comparisons between counts of reads obtained from ST-RIG-I or ST-MDA5 vs negative control (ST-CH) from three independent replicates (R1; R2; and R3). Non-significant (n.s.) were indicated. *p < 0.05, **p < 0.01, ***p < 0.001, ****P < 0.0001.

abundance of reads (coverage) of either RIG-I or MDA5-ligands by the mean read coverage of their total input sample, ii) the RLRs read coverage to read coverage obtained with the mCherry negative control. NGS data analysis failed to show RLR association with viral RNAs upon Tha infection in our experimental conditions (Fig. 3A).

Interestingly, the NGS study of the RABV vaccine strain, SAD, showed a significant coverage and much higher enrichment in MDA5 associated with the whole negative-sense genomic RNA than with the positive-sense antigenome, suggesting that MDA5 may be engaged in SAD RNAs recognition, specifically on the negative-

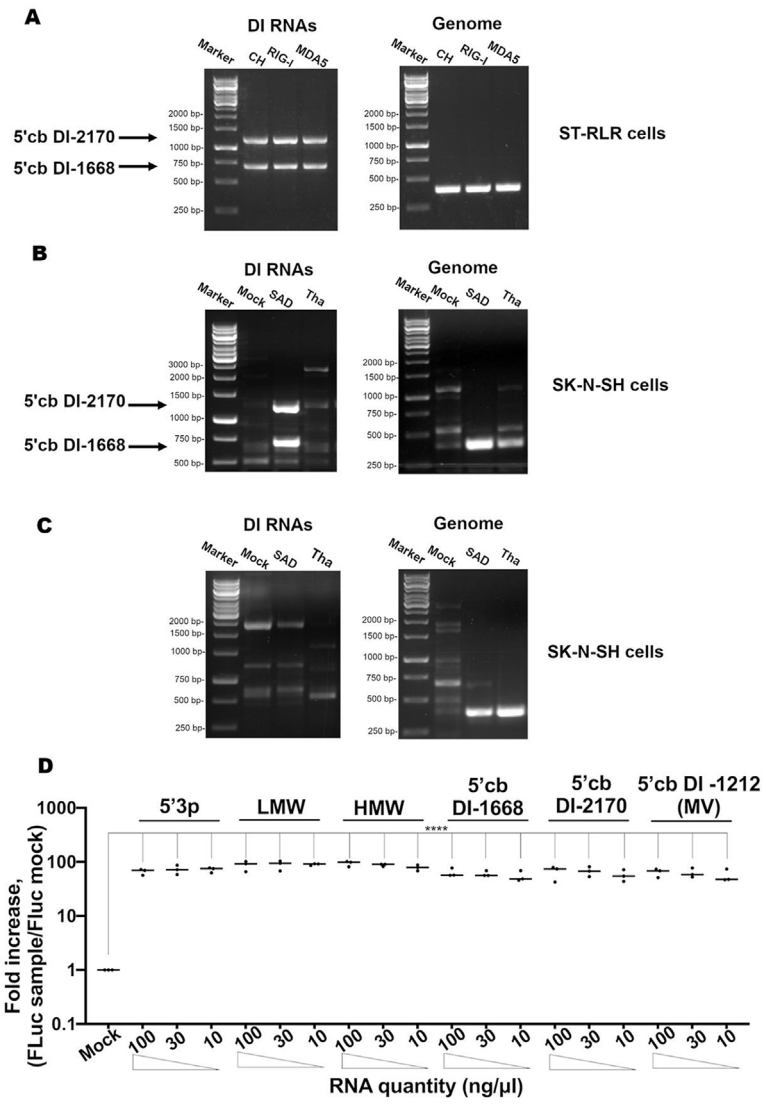

Fig. 4. Characterization and functional validation of SAD 5′ cb DI viral genomes: A. Detection of 5′cb DI-1668 (707bp), 5′cb DI-2170 (1209 bp) (left panel), and SAD genome (400 bp, right panel) by RT-PCR on total RNAs extracted from SAD-infected ST-CH, ST-RIG-I, and ST-MDA5 at an MOI of 0.5 for 24 h. B. Detection of 5′cb DI-1668, 5′cb DI-2170 (left panel), SAD, and Tha genomes (right panel) by RT-PCR on total RNAs extracted from SAD or Tha infected neuroblastoma cells (SK-N-SH) at an MOI of 0.5 for 24h using universal 5′ cb primers (1 and 2) and full-length genome primers (2 and 3) (Table S7). C. RT-PCR on 2 µg of total RNAs extracted from SAD or Tha-infected neuroblastoma cells (SK-N-SH) at an MOI of 0.5 for 24h using Tha-optimized 5′ cb DI primers (4 and 5) (left panel) and Tha-optimized full-length genome (3 and 4) primers (right panel) (Table S7). D. Luciferase expression in ISRE-reporter cells transfected with 100, 30, or 10 ng/µl of i) synthetic RNAs: 5′3P, LMW poly(I:C), HMW poly(I:C), or ii) 5′cb DI-1668, and 5′cb DI-2170 (Table S6) or, iii) 5′cb DI-1212 RNAs MV (measles virus) used as a positive control [14]. For all experiments, three biological replicates were performed and data are represented as a median. The results are represented as a fold increase of ISRE expression compared to mock non-transfected cells. P values were calculated by comparing each experimental condition to mock non-transfected cells using one-way ANOVA with Tukey's multiple comparisons. *p < 0.05, **p < 0.01, ***p < 0.001, ****P < 0.0001.

sense genome (Fig. 3B). These results are in contrast with previous analysis of RNA bound to MDA5 in measles virus-infected cells (also negative-sense single-stranded RNA virus) reported MDA5 interaction only with positive-strand viral RNA [12,15]. However, despite viral RNA/MDA5 interaction, we failed to observe any statistically significant induction of ISRE promoter by MDA5-specific RABV RNA ligands in our ISRE reporter assay (Fig. 2D).

Analysis of RIG-I-specific RNA ligands purified from SAD-infected cells revealed a significant enrichment of negative- and positive-sense viral RNAs (Fig. 3B) and in particular the 5′ and 3' extremities of genomic and antigenomic RNAs, respectively. These results are in concordance with both the RLR silencing experiment (Fig. 1) and the statistically significant stimulation of the ISRE promoter by the SAD RNAs, which are bound to RIG-I (Fig. 2D), further suggesting that RIG-I is the main actor in recognizing RABV RNA.

Since the three independent experiments show some variability in RIG-I and MDA5 enrichment (Fig. 3B and C, green and orange lines), principal component analysis (PCA) of each biological replicate was performed to visualize trends across the three datasets obtained with Tha and SAD strains (Fig. S2). For Tha, the PCA analysis failed to properly distinguish the clean separation of biological samples, whereas, for SAD, the PCA plots showed that the main source of variability along dimension 1 corresponded to the

clustering of ST-RIG-I and ST-MDA5 samples from the ST-CH sample (Fig. S2B). This explains 80% of the variability, confirming that RNAs bound to RIG-I and MDA5, upon SAD infection, were different from RNAs bound to the mCherry negative control.

To further explore the RNA primary sequence of viral RLR ligands that could explain SAD RNA recognition by RIG-I and MDA5, we analyzed the AU-rich content sequence of RIG-I and MDA5-specific reads (Fig. S3). We observed that MDA5 binding to SAD negative-sense genomic RNAs correlated with high AU-rich content (> AU content of SAD genome 0.55) ($p < 0.001$, Cohen's $d = -0.53$) (Fig. S3D). However, RIG-I-SAD negative-sense ligands were characterized by a lower AU-rich content sequence than that observed for MDA5 ligands, suggesting that RIG-I binding did not correlate with RNA primary sequence (Fig. S3B). For the positive-strand SAD RNA species, we did not detect any preference for the binding of AU-rich regions by RIG-I or MDA5 (Figs. S3A and C). In conclusion, our results suggest preferential binding of MDA5 to AU-rich regions of viral genomes as compared to RIG-I, which did not interact with AU-rich sequences.

In a recent work, we demonstrated an important role of conserved endogenous RNA in the activation of RIG-I signaling upon infection with various RNA viruses [34]. Here, we performed an additional analysis of RNAseq results to detect statistically enriched endogenous RNA ligands on RIG-I in RABV-infected cells. As reported by Vabret et al. [14,15,33,34], we detected several RNAs transcribed by Polymerase III such as, small noncoding Y RNAs: RNY4 statistically enriched on the RIG-I sensor for both Tha and SAD infections (Table S2). In addition, RNY1 and VTRNA1-1 were detected in the ST-RIG-I output sample when cells were infected by the SAD strain. Corresponding total RNA NGS results were controlled, validating the lack of differences in the transcription efficiency of these endogenous RNAs (Table S3).

To determine whether Tha and SAD infection trigger different ISG signatures, NGS data were analyzed to compare the ISG expression in total RNAs extracted from ST-RLR cells upon Tha or SAD infections. In comparison to ST-CH cells, ST-RIG-I Tha- or SAD-infected cells showed high expression of the DDX58 gene (Table S4) thus validating the RIG-I overexpression. Interestingly, Tha and SAD replications in ST-RIG-I cells induced significant up-regulation of three ISGs (DUSP5, GPMR, and PRAME, Table S4). Compared to Tha, SAD infection induced statistically significant up-regulation of sixteen ISGs (EPSTI1, BST2, IFI16, IFI35, IFI44L, IFI6, IFITM2, IFITM3, IRF7, ISG15, OAS2, STAT1, STAT2, TAP1, PML, and UBE2L6; Table S4). However, compared to ST-CH in ST-MDA-5 cells only the IFIH1, MDA-5 coding gene, expression was up-regulated thus validating the MDA-5 cell line. No differences in ISG expression were observed in ST-MDA-5 cells infected with either Tha or SAD viruses (Data not shown). The expression of housekeeping genes in ST-RIG-I remained stable upon infection (Table S5).

Thus, we observed that the RIG-I receptor detected RABV RNA but only when cells were infected with the vaccine SAD strain. NGS data analysis of RLR-specific RNAs upon RABV infection suggested that the 5′-end extremity of the genome and 3′-end extremity of antigenome would play an important role in the immune stimulation of ISGs expression induced by the SAD vaccine strain. For both wild-type and vaccine RABV strains, self-RNA transcribed by Polymerase III interacted with RIG-I.

3.5. Characterization of RIG-I-specific SAD 5′cb DI viral genomes

We asked whether RIG-I specific negative- and positive-RNA ligands observed during SAD infection (Fig. 3B) could be attributed to 5′ cb DI viral genomes since 5′ cb DI viral genomes are known to be strong RIG-I agonists [13–15]. To do this, we applied the DI-tector algorithm to search for the presence of 5′cb DI viral genomes in Tha and SAD NGS datasets [37]. We failed to detect any 5′cb DI genome in ST-RLR cells infected with Tha cells. Interestingly, using the DI-tector, we identified two 2170- and 1668-nucleotide-long 5′ cb DI viral genomes in SAD-infected cells (Table 1). 5′cb DI-1668 exhibited statistically significant ($p = 0.04$) read abundance in the RIG-I output samples as compared to the negative control ST-CH. The enrichment of 5′cb DI-2170 on RIG-I, on the other hand, failed to be statistically validated (Table 1).

We further studied the molecular organization of the detected 5′cb DI-2170 and 5′cb DI-1668 DI viral genomes and juxtaposed them in Fig. 3B with SAD RIG-I/RNA NGS data represented. 5′cb DI-2170 resulted from a breakpoint (BP) at position 9823 of the full-length viral genome and re-initiation (RI) at position 11865. 5′cb DI-1668 generated from a BP position at 10898 and RI at position 11292 (Table 1, Fig. 3C). Complete DI-genome sequences are indicated in Table S6. We observed that both negative- and positive-sense 5′cb DI viral genomes were enriched on RIG-I in SAD-infected cells (Fig. 3B). Indeed, similar to the full-length viral genome, 5′cb DI genomes replicated *via* the production of anti-genomes. 5′ cb DI viral genomes were characterized by the presence of a sequence with a perfect complementarity at both RNA ends which hybridized, forming a stem-loop structure (Fig. S4) that has been shown to stimulate RIG-I [4,13–15].

Our data demonstrates for the first time the lack of a detectable amount of cb DI viral genomes in the RABV field isolate (Tha) which may confirm the outcome of viral infection. However, the live-attenuated SAD vaccine strain presents an important source of 5′cb immunogenic RNAs recognized *via* the RIG-I.

3.6. Validation of 5′cb DI viral genomes production by RABV SAD strain using a conventional approach

To further validate the presence of 5′cb DI viral genomes in SAD-infected ST-RLR cells, we applied a universal RT-PCR analysis on total RNA extracted from ST-RLR cells infected with SAD at an MOI of 0.5 for 24h. Using universal 5′cb DI genome-specific primers as described previously [14,38], two DNA fragments were detected on agarose gel of approximately 0.7 Kb and 1.2 Kb corresponding to 5′cb DI-1668 and 5′cb DI-2170, respectively (Fig. 4A). Additionally, Sanger sequencing of the two amplicons confirmed the characteristics of the 5′ cb DI genomes i.e., BP and RI sites (Table S6). Furthermore, the presence of 5′cb DI genomes was examined in human neuroblastoma cells (SK-N-SH), a more relevant cell model to study RABV infection and pathogenesis. These cells were infected with either RABV field isolate Tha or RABV vaccine strain SAD. Using 5′ cb DI genomes' universal primers, only SAD-infected cells demonstrated the presence of two PCR fragments corresponding to DI-1668 and DI-2170 (Fig. 4B) which was further validated by Sanger sequencing. Furthermore, we failed to detect any 5′cb DI genomes from Tha-infected cells using optimized Tha-specific primers (Fig. 4C). Thus, RT-PCR analysis of 5′ cb DI viral genomes in SK-N-SH cells corroborated the DI-tector study performed on our NGS data (Fig. 3). Moreover, these experiments validated the presence of identical 5′cb DI viral genomes produced independently of the cell type in SAD-infected ST-RLR and human neuroblastoma cells.

To analyze the immunostimulatory properties of RABV 5′cb, we generated *in vitro* transcribed DI-1668 and DI-2170 and measured type-I IFN signaling using our ISRE reporter cell line. Similarly to the RLR-specific synthetic (5′3P RNA, HMW, and LMW poly(I:C)) and natural measles virus 5′cb DI-1212 agonists [14,39], RABV 5′ cb DI-1668 and DI-2170 induced a comparable ISRE promoter activation (Fig. 4D).

These experiments corroborate the NGS results of RIG-I-specific RNA ligands in RABV-infected cells, the DI-tector analysis and

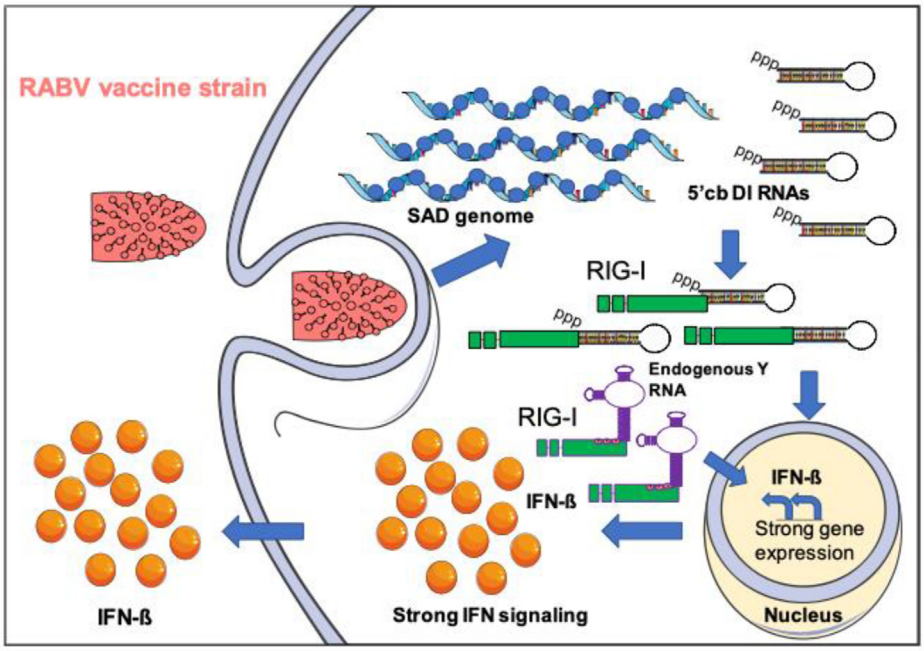

Fig. 5. Model of SAD RNAs recognition by RIG-I and modulation of IFN response. During cells' infection with the vaccine, the SAD strain, viral genome and 5′cb DI RNAs are replicated in the cytoplasm. 5′cb DI RNAs are then detected by the RIG-I sensor triggering a signaling cascade that activates a strong IFN response.

confirm our findings that RABV 5′cb DI RNAs are strongly immunoactive.

4. Discussion

RLRs cytosolic sensors are the first line of defense that trigger the innate immune response by detecting viral RNAs in cytoplasm. Therefore, understanding the RLR signaling could help develop antiviral therapeutics that control viral infection. Further, it could shed light on some of the mechanisms explaining the attenuation of some viruses. Several studies have performed characterization of RNA partners bound to RLRs within infected cells using various riboproteomic approaches. RNAs bound to RLRs were isolated by Co-IP or tagged-protein affinity purification and then characterized by NGS. Using these approaches, first RIG-I-specific RNA partners for negative-sense RNA viruses (Sendai, influenza, VSV, and Measles viruses) and positive-sense RNA viruses (Dengue, Zika viruses, Chikungunya) were identified [4,12,13,15,33].

RABV is thought to counteract IFN induction and inflammation in many ways [40]. Indeed, mice infected with attenuated RABV had stronger inflammatory reactions than mice infected with the wild-type RABV [41]. However, a previous study of RABV RNA recognition, completed in the absence of productive infection, was performed by transfecting cells with *in vitro* transcribed RNA or RNAs coming from RABV-infected cells [9]. Therefore, we lack a deeper understanding of real RNA signatures recognized by RLRs during RABV infection. In our study, we addressed this question in the presence of active infection by comparing two RABV strains: cell culture-adapted canine RABV field isolate from Thailand (Tha) and a RABV vaccine strain (SAD) used largely to produce live-attenuated and inactivated vaccine stocks.

We demonstrated that RNA molecules isolated from Tha- or SAD-infected cells induced ISRE and IFN-β expression. However, we observed that the induction of ISRE was different for the two strains. Specifically, the vaccine induced a stronger IFN response than the wild-type. Further, silencing of either RIG-I or MDA5 suggested that RIG-I was the major RLR for Tha or SAD viral strains. These observations are in agreement with previous work indicating that RIG-I is required for the initiation of an IFN response upon cell infection with recombinant RABV vaccine strain SAD-L16 [9]. In addition, the LGP2 overexpression inhibited the IFN-β expression in ST-LGP2 cells transfected with RABV RNAs, confirming RIG-I's role in RNA detection. Our results are in line with previous studies on the involvement of RIG-I in the detection of negative-sense RNA viruses (Sendai virus, Measles virus, and Influenza virus) [4,12,13,15,33,42]. More specifically, the results obtained with RABV are in agreement with the previously described study performed on Vero cells transfected with plasmids coding either for a full-length or a truncated (dominant-negative mutant, RIG-IC) RIG-I and infected with SAD-L16 strain [9].

Using an RLR/RNA pull-down approach coupled with NGS, we detected an enrichment of 5′ cb DI genomes of both negative- and positive-sense in our RIG-I-specific RNA samples and only in SAD-infected cells but not in the field isolate Tha. Interestingly, for the measles virus, only the modified recombinant virus produced 5′ cb DI-RNAs upon cell infection. The vaccine MV-Schwarz strain, on the other hand, did not produce 5' cb DI-RNAs upon cell infection [14].

Moreover, we found evidence of an interaction between the full-length genome and the MDA5 in SAD-infected cells. However, we failed to detect any immunostimulation activity of MDA5-specific RNA partners in our type-I IFN reporter assays. *In silico* analysis showed that the genomic sequence of SAD bound to MDA5 presented an AU-rich composition. It has been reported that the AU-rich RNA species bound to MDA5 are poorer activators of ATP hydrolysis of MDA5 *in vitro*, forming a stable MDA5 filament structure [12]. This feature may explain the lack of immunostimulatory activity of the MDA5-SAD ligands due to their AU-rich composition reported in our study. However, this observation may be cell-specific as RABV was previously shown to induce IFN in dendritic cells of RIG-I knockout mice, suggesting that MDA5 could be in that particular case involved in RABV sensing upon infection [43].

Interestingly, we failed to detect any specific RABV RNA ligands upon infection with the Tha strain (Fig. 3A) but did detect significant immunostimulation activity of total RNA from Tha-infected cells and RNAs collected from the RIG-I pull-down (Figs. 1 and 2C). Our NGS data analysis provided evidence of enrichment in 5′3P endogenous noncoding RNA ligands (RNY4, RNY1, RN7SL674P, RN7SL767P, VTRNA1-1) on RIG-I upon infection with Tha or SAD RABVs (Table S2). We have previously observed that a large spectrum of RNA virus infections leads to the mobilization of endogenous RNA ligands (transcripts of RNA Polymerase III) on RIG-I that activates RIG-I signaling pathways even in the absence of RIG-I-specific viral RNA ligands [34].

Different viruses are targeted by unique sets of ISGs. To address this question for RABV infection, ISG expression was analyzed in ST-CH, ST-RIG-I, and ST-MDA-5 cells. Three ISGs were up-regulated in ST-RIG-I cells upon Tha or SAD replication (DUSP5, GPMR, and PRAME, Table S4). Further, ST-RIG-I cells showed statistically significant up-regulation of sixteen ISGs induced only upon SAD vaccine strain replication (EPSTI1, BST2, IFI16, IFI35, IFI44L, IFI6, IFITM2, IFITM3, IRF7, ISG15, OAS2, STAT1, STAT2, TAP1, PML, and UBE2L6; Table S4). Interestingly, when compared to the ST-CH, no ISG expression was induced by Tha or SAD infections of ST-MDA-5 cells thus confirming that RIG-I is the main sensor upon RABV infection. Studies on ISG's ability to inhibit viral replication have been performed [44]. In these studies, IFI16 directly senses viral RNA and enhances RIG-I transcription and activation to restrict influenza virus infection [45]. However, many ISGs play a negative role in innate immune response modulation induced after virus infection. Studies on VSV replication show that IFI35 depletion led to reduced VSV replication. In addition, IFI35 suppresses i) IFN-β and ISG56 promoters ii) dephosphorylation (activation) of the RIG-I sensor [46]. IFI44L expression showed a novel function in innate immune modulation. Indeed, a decrease in IFI44L expression impairs virus production, and IFI44L expression negatively impacts the antiviral state induced by an analog of dsRNA or by an IFN treatment [47].

DI viral genomes or defective viral genomes (DVG) are generated upon virus replication in cells, producing defective viral particles that are biochemically and morphologically similar to standard virus particles but harbor deletions in their genomes [48]. DVGs are known to replicate by the viral polymerase of a helper (full-length genome) virus, interfering with its production [16,48].

DVGs were isolated from a broad range of negative-sense RNA viruses including VSV, Sendai virus, Measles virus, and Influenza A virus (recently reviewed in Ref. [48]). Further, DVG particles have also been found in human natural infections and correlated with the course of the disease [49]. Indeed, genomic analysis of Influenza A virus (H1N1) isolated from a cohort with severe and in some cases fatal outcomes identified few DVG, while isolates from a mild case of disease produced a high level of them. This suggests that DVG is a new virulence marker for the viral pathogenicity [50]. In the case of RABV, DVG particles were also observed *in vivo* in newborn mice brains inoculated intracerebrally with the highly attenuated RABV HEP Flury strain or VSV [51].

In summary, using the riboproteomic approach coupled with NGS, we show molecular signature of RIG-I and MDA5-specific RNA ligands upon infection with RABV. Our results show a significant positive correlation between 5′ cb DIs and the strong RIG-I mediated IFN response that can be attributed to the efficient activation of the immune response by the RABV vaccine SAD strain (Fig. 5). Our results suggest that 5' cb DIs production by a live-attenuated RNA virus vaccine strain can serve as a marker of its immunostimulatory properties, which positively correlates with vaccine efficacy.

Declaration of competing interest

The authors declare no competing interests.

Acknowledgments

We acknowledge all the members of the Lyssavirus, epidemiology, and neuropathology team and the Vaccines-innovation laboratory at Pasteur Institute for their help and useful discussions.

We thank the members of the Biomics platform at Institut Pasteur for providing advice for NGS experiments. We thank Alexis Criscuolo and Vincent Guillemot (Hub Bioinformatique et Biostatistique, Institut Pasteur) for help with analysis. We are grateful to Katherine Worsley-Tonks for a critical reading of the manuscript.

This study was supported by ANR- 16-CE11-0031-01, the Institut Pasteur, and the CNRS.

Appendix A. Supplementary data

Supplementary data to this article can be found online at https://doi.org/10.1016/j.micinf.2024.105321.

References

[1] Beutler B, Rietschel ET. Innate immune sensing and its roots: the story of endotoxin. Nat Rev Immunol 2003;3:169–76. https://doi.org/10.1038/nri1004.

[2] Sanchez David RY, Combredet C, Najburg V, Millot GA, Beauclair G, Schwikowski B, et al. LGP2 binds to PACT to regulate RIG-I– and MDA5-mediated antiviral responses. Sci Signal 2019;12:1–14. https://doi.org/10.1126/scisignal.aar3993.

[3] Bruns AM, Leser GP, Lamb RA, Horvath CM. The innate immune sensor LGP2 activates antiviral signaling by regulating MDA5-RNA interaction and filament assembly. Mol Cell 2014;55:771–81. https://doi.org/10.1016/j.molcel.2014.07.003 [The].

[4] Linder A, Bothe V, Linder N, Schwarzlmueller P, Dahlström F, Bartenhagen C, et al. Defective interfering genomes and the full-length viral genome trigger RIG-I after infection with vesicular stomatitis virus in a replication dependent manner. Front Immunol 2021;12:1–17. https://doi.org/10.3389/fimmu.2021.595390.

[5] Rehwinkel J, Gack MU. RIG-I-like receptors: their regulation and roles in RNA sensing. Nat Rev Immunol 2020;20:537–51. https://doi.org/10.1038/s41577-020-0288-3.

[6] Deddouche S, Goubau D, Rehwinkel J, Chakravarty P, Begum S, Maillard PV, et al. Identification of an LGP2-associated MDA5 agonist in picornavirus-infected cells. Elife 2014;3:1–20. https://doi.org/10.7554/elife.01535.

[7] Yin X, Riva L, Pu Y, Martin-Sancho L, Kanamune J, Yamamoto Y, et al. MDA5 governs the innate immune response to SARS-CoV-2 in lung epithelial cells. Cell Rep 2021;34:1–11. https://doi.org/10.2139/ssrn.3682826.

[8] Schuberth-Wagner C, Ludwig J, Bruder AK, Herzner AM, Zillinger T, Goldeck M, et al. A conserved histidine in the RNA sensor RIG-I controls immune tolerance to N1-2'O-methylated self RNA. Immunity 2015;43:41–51. https://doi.org/10.1016/j.immuni.2015.06.015.

[9] Hornung V, Kato H, Poeck H, Akira S, Conzelmann K, Schlee M. 5'-triphosphate RNA is the ligand for RIG-I. Science 2006;314(80-):994–7.

[10] Pichlmair A, Schulz O, Tan C-P, Rehwinkel J, Kato H, Takeuchi O, et al. Activation of MDA5 requires higher-order RNA structures generated during virus infection. J Virol 2009;83:10761–9. https://doi.org/10.1128/jvi.00770-09.

[11] Wu B, Peisley A, Richards C, Yao H, Zeng X, Lin C, et al. Structural basis for dsRNA recognition, filament formation, and antiviral signal activation by MDA5. Cell 2013;152:276–89. https://doi.org/10.1016/j.cell.2012.11.048.

[12] Runge S, Sparrer KMJ, Lässig C, Hembach K, Baum A, García-Sastre A, et al. In vivo ligands of MDA5 and RIG-I in measles virus-infected cells. PLoS Pathog 2014;10:1–13. https://doi.org/10.1371/journal.ppat.1004081.

[13] Baum A, Sachidanandam R, García-Sastre A. Preference of RIG-I for short viral RNA molecules in infected cells revealed by next-generation sequencing. Proc Natl Acad Sci USA 2010;107:16303–8. https://doi.org/10.1073/pnas.1100561108.

[14] Mura M, Combredet C, Najburg V, Sanchez David RY, Tangy F, Komarova AV. Nonencapsidated 5'Copy-back defective interfering genomes produced by recombinant measles viruses are recognized by RIG-I and LGP2 but not MDA5. J Virol 2017;91:1–22.

[15] Sanchez David RY, Combredet C, Sismeiro O, Dillies MA, Jagla B, Coppée JY, et al. Comparative analysis of viral RNA signatures on different RIG-I-like receptors. Elife 2016;5:1–27. https://doi.org/10.7554/eLife.11275.

[16] Lazzarini RA, Keene JD, Schubert M. The origins of defective interfering particles of the negative-strand RNA viruses. Cell 1981;26:145–54. https://doi.org/10.1016/0092-8674(81)90298-1.
[17] Hampson K, Coudeville L, Lembo T, Sambo M, Kieffer A, Attlan M, et al. Estimating the global burden of endemic canine rabies. PLoS Neglected Trop Dis 2015;9:e0003709. https://doi.org/10.1371/journal.pntd.0003709.
[18] Masatani T, Ito N, Shimizu K, Ito Y, Nakagawa K, Sawaki Y, et al. Rabies virus nucleoprotein functions to evade activation of the RIG-I-mediated antiviral response. J Virol 2010;84:4002–12. https://doi.org/10.1128/jvi.02220-09.
[19] Masatani T, Ito N, Ito Y, Nakagawa K, Abe M, Yamaoka S, et al. Importance of rabies virus nucleoprotein in viral evasion of interferon response in the brain. Microbiol Immunol 2013;57:511–7. https://doi.org/10.1111/1348-0421.12058.
[20] Rieder M, Brzo K, Pfaller CK, Cox JH, Stitz L, Conzelmann K. Genetic dissection of interferon-antagonistic functions of rabies virus phosphoprotein : inhibition of interferon regulatory factor 3 activation is important for pathogenicity. J Virol 2011;85:842–52. https://doi.org/10.1128/JVI.01427-10.
[21] Harrison AR, Lieu KG, Larrous F, Ito N, Bourhy H, Moseley GW. Lyssavirus P-protein selectively targets STAT3-STAT1 heterodimers to modulate cytokine signalling. PLoS Pathog 2020;16:1–23. https://doi.org/10.1371/JOURNAL.PPAT.1008767.
[22] Wiltzer L, Larrous F, Oksayan S, Ito N, Marsh GA, Wang LF, et al. Conservation of a unique mechanism of immune evasion across the. J Virol 2012;86:10194–9. https://doi.org/10.1128/JVI.01249-12.
[23] Hossain MA, Larrous F, Rawlinson SM, Zhan J, Sethi A, Ibrahim Y, et al. Structural elucidation of viral antagonism of innate immunity at the STAT1 interface. Cell Rep 2019;29:1934–1945.e8. https://doi.org/10.1016/j.celrep.2019.10.020.
[24] Ben Khalifa Y, Luco S, Besson B, Sonthonnax F, Archambaud M, Grimes JM, et al. The matrix protein of rabies virus binds to RelAp43 to modulate NF-κB-dependent gene expression related to innate immunity. Sci Rep 2016;6:1–13. https://doi.org/10.1038/srep39420.
[25] Besson B, Sonthonnax F, Duchateau M, Khalifa Y Ben, Matondo M, Chamot J, et al. Regulation of NF- κ B by the p105-ABIN2-TPL2 complex and RelAp43 during rabies virus infection. PLoS Pathog 2017;13:1–24.
[26] Sonthonnax F, Bess B, Bonnaud E, Jouvion G, Merino D, Larrous F, et al. Lyssavirus matrix protein cooperates with phosphoprotein to modulate the Jak-Stat pathway. Sci Rep 2019;9:1–13. https://doi.org/10.1038/s41598-019-48507-4.
[27] Liang B, Li Z, Jenni S, Rahmeh AA, Morin BM, Grant T, et al. Structure of the L protein of vesicular stomatitis virus from electron cryomicroscopy. Cell 2015;162:314–27. https://doi.org/10.1016/j.cell.2015.06.018.
[28] Horwitz JA, Jenni S, Harrison SC, Whelan SPJ. Structure of a rabies virus polymerase complex from electron cryo-microscopy. Proc Natl Acad Sci U S A 2020;117:2099–107. https://doi.org/10.1073/pnas.1918809117.
[29] Tian D, Luo Z, Zhou M, Li M, Yu L, Wang C, et al. Critical role of K1685 and K1829 in the large protein of rabies virus in viral pathogenicity and immune evasion. J Virol 2016;90:232–44. https://doi.org/10.1128/JVI.02050-15.
[30] Thiel V, Sen GC, Fensterl V, Klimstra WB, Pierson TC, Buller RM, et al. mRNA cap methylation influences pathogenesis of vesicular. J Virol 2014;88:2913–26. https://doi.org/10.1038/nature09489.
[31] Muthukrishnan S, Both GW, Furuichi Y, Shatkin AJ. mRNA is required for translation. Nature 1975;255:33–5.
[32] Züst R, Cervantes-Barragan L, Habjan M, Maier R, Neuman BW, Ziebuhr J, et al. Ribose 2'-O-methylation provides a molecular signature for the distinction of self and non-self mRNA dependent on the RNA sensor MDA5. Nat Immunol 2011;12:137–43. https://doi.org/10.1038/ni.1979.
[33] Chazal M, Beauclair G, Ségolène G, Valérie N, Etienne S-L, Frédéric T, et al. RIG-I recognizes the 5' region of dengue and Zika virus genomes. Cell Rep 2018;24:320–8. https://doi.org/10.1016/j.celrep.2018.06.047.
[34] Vabret N, Najburg V, Solovyov A, Gopal R, McClain C, Šulc P, et al. RNAs are conserved endogenous RIG-I ligands across RNA virus infection and are targeted by HIV-1. iScience 2022;25:104599. https://doi.org/10.1016/j.isci.2022.104599.
[35] Lucas-Hourani M, Dauzonne D, Jorda P, Cousin G, Lupan A, Helynck O, et al. Inhibition of pyrimidine biosynthesis pathway suppresses viral growth through innate immunity. PLoS Pathog 2013;9:1–18. https://doi.org/10.1371/journal.ppat.1003678.
[36] Quinlan AR, Hall IM. BEDTools: a flexible suite of utilities for comparing genomic features. Bioinformatics 2010;26:841–2. https://doi.org/10.1093/bioinformatics/btq033.
[37] Beauclair G, Mura M, Combredet C, Tangy F, Jouvenet N, Komarova AV. DI-tector: defective interfering viral genomes' detector for next-generation sequencing data. RNA 2018;24:1285–96. https://doi.org/10.1261/rna.066910.118.
[38] Pfaller CK, Radeke MJ, Cattaneo R, Samuel CE. Measles virus C protein impairs production of defective copyback double-stranded viral RNA and activation of protein kinase R. J Virol 2014;88:456–68. https://doi.org/10.1128/jvi.02572-13.
[39] Komarova AV, Combredet C, Sismeiro O, Dillies MA, Jagla B, David RYS, et al. Identification of RNA partners of viral proteins in infected cells. RNA Biol 2013;10:943–56. https://doi.org/10.4161/rna.24453.
[40] Faul EJ, Lyles DS, Schnell MJ. Interferon response and viral evasion by members of the family rhabdoviridae. Viruses 2009;1:832–51. https://doi.org/10.3390/v1030832.
[41] Wang ZW, Sarmento L, Wang Y, Li X, Dhingra V, Tseggai T, et al. Attenuated rabies virus activates, while pathogenic rabies virus evades, the host innate immune responses in the central nervous system. J Virol 2005;79:12554–65. https://doi.org/10.1128/jvi.79.19.12554-12565.2005.
[42] Rehwinkel J, Tan CP, Goubau D, Schulz O, Pichlmair A, Bier K, et al. RIG-I detects viral genomic RNA during negative-strand RNA virus infection. Cell 2010;140:397–408. https://doi.org/10.1016/j.cell.2010.01.020. https://doi.org/S0092-8674(10)00021-8[pii]\r.
[43] Faul EJ, Wanjalla CN, Suthar MS, Jr MG, Wirblich C, Schnell MJ. Rabies virus infection induces type I interferon production in an IPS-1 dependent manner while dendritic cell activation relies on IFNAR signaling. PLoS Pathog 2010;6:1–15. https://doi.org/10.1371/journal.ppat.1001016.
[44] Schoggins JW, Wilson SJ, Panis M, Murphy MY, Jones CT, Bieniasz P, et al. A diverse array of gene products are effectors of the type I interferon antiviral response. Nature 2011;472:481–5. https://doi.org/10.1038/nature09907.A.
[45] Jiang Z, Wei F, Zhang Y, Wang T, Gao W, Yu S, et al. IFI16 directly senses viral RNA and enhances RIG-I transcription and activation to restrict influenza virus infection. Nat Microbiol 2021;6:932–45. https://doi.org/10.1038/s41564-021-00907-x.
[46] Das A, Dinh PX, Panda D, Pattnaik AK. Interferon-inducible protein IFI35 negatively regulates RIG-I antiviral signaling and supports vesicular stomatitis virus replication. J Virol 2014;88:3103–13. https://doi.org/10.1128/jvi.03202-13.
[47] DeDiego ML, Martinez-Sobrido L, Topham DJ. Novel functions of IFI44L as a feedback regulator of host antiviral responses. J Virol 2019;93:1–21.
[48] Ziegler CM, Botten JW. Defective interfering particles of negative-strand RNA viruses. Trends Microbiol 2020;28:554–65. https://doi.org/10.1016/j.tim.2020.02.006.
[49] Sun Y, Jain D, Koziol-White CJ, Genoyer E, Gilbert M, Tapia K, et al. Immunostimulatory defective viral genomes from respiratory syncytial virus promote a strong innate antiviral response during infection in mice and humans. PLoS Pathog 2015;11:1–21. https://doi.org/10.1371/journal.ppat.1005122.
[50] Vasilijevic J, Zamarreño N, Oliveros JC, Rodriguez-Frandsen A, Gómez G, Rodriguez G, et al. Reduced accumulation of defective viral genomes contributes to severe outcome in influenza virus infected patients. PLoS Pathog 2017;13:1–29. https://doi.org/10.1371/journal.ppat.1006650.
[51] Holland JJ, Villarreal LP. Purification of defective interfering T particles of vesicular stomatitis and rabies viruses generated in vivo in brains of newborn mice. Virology 1975;67:438–49. https://doi.org/10.1016/0042-6822(75)90445-6.